

Orientation and quasar black hole mass estimation

Michael S. Brotherton^{1*}, Vikram Singh¹, Jessie Runnoe²

¹*Department of Physics and Astronomy, University of Wyoming, Laramie, WY 82071, USA*

²*Department of Astronomy and Astrophysics, The Pennsylvania State University
525 Davey Lab, University Park, PA 16803, USA*

ABSTRACT

We have constructed a sample of 386 radio-loud quasars with $z < 0.75$ from the Sloan Digital Sky Survey in order to investigate orientation effects on black hole mass estimates. Orientation is estimated using radio core dominance measurements based on FIRST survey maps. Black hole masses are estimated from virial-based scaling relationships using $H\beta$, and compared to the stellar velocity dispersion (σ_*), predicted using the Full Width at Half Maximum (FWHM) of [O III] $\lambda 5007$, which tracks mass via the $M-\sigma_*$ relation. We find that the FWHM of $H\beta$ correlates significantly with radio core dominance and biases black hole mass determinations that use it, but that this is not the case for σ_* based on [O III] $\lambda 5007$. The ratio of black hole masses predicted using orientation-biased and unbiased estimates, which can be determined for radio-quiet as well as radio-loud quasars, is significantly correlated with radio core dominance. Although there is significant scatter, this mass ratio calculated in this way may in fact serve as an orientation estimator. We additionally note the existence of a small population radio core-dominated quasars with extremely broad $H\beta$ emission lines that we hypothesise may represent recent black hole mergers.

Key words: galaxies: active – quasars: general.

1 INTRODUCTION

Quasars are not spherically symmetric systems. This is most apparent in the large-scale radio jets present in a minority of sources, but several inferred quasar structures, notably accretion disks and dusty torii, are also axisymmetric. In radio-loud quasars, radio core dominance and spectral indices can be used to estimate system orientation (Orr & Browne 1982; Wills & Brotherton 1995; Van Gorkom et al. 2015). There is as yet no reliable orientation indicator for radio-quiet quasars, which represent about 90% of all quasars (but see Boroson 2011 and Sulentic et al. 2012).

This axisymmetry is important to understand and account for when estimating some fundamental quasar parameters, such as black hole mass. Many methods of determining quasar black hole mass (e.g., Shen 2013, Peterson 2011) depend on the assumption of virial motion and use the Doppler-broadened velocity width of an emission line – usually $H\beta$ at low redshift. The broad $H\beta$ emission-line width, often characterized by the Full Width at Half Maximum or FWHM, however, is correlated with orientation indicators in radio-loud quasars (e.g., Wills & Browne 1986). This is suggestive that at least part of the broad-line region

(BLR) is flattened into a disk, with edge-on systems showing the broadest lines, a conclusion also supported by other lines of evidence (Gaskell 2009a). The velocity width of lines like $H\beta$ are apparently related to both black hole mass and system orientation.

Runnoe et al. (2013) compared black hole masses computed using single-epoch (SE) scaling relationships (e.g., Vestergaard & Peterson 2006) for both $H\beta$ and C IV $\lambda 1549$, the latter lacking strong FWHM changes with orientation (but see Runnoe et al. 2014 for a discussion of some subtle profile changes). They found that the difference in the two black hole mass estimates significantly correlated with radio-based orientation parameters and determined correction terms for the $H\beta$ -based formula. The same orientation effects affecting $H\beta$ also appear to be present in radio-quiet quasars (Shen & Ho 2014). It would be valuable to be able to provide an estimation of orientation for all quasars, not just radio-loud objects, to better determine how quasar properties change with viewing angle.

Another method exists for estimating black hole mass in quasars, via the correlation with stellar velocity dispersion σ_* (e.g., Gebhardt et al. 2000; Ferrarese & Merritt 2000). The so-called $M-\sigma_*$ relation, present in both active and quiescent galaxies, may represent an important clue to galaxy evolution. In the majority of quasars, the continuum

* E-mail: mbrother@uwyo.edu

dilutes the stellar absorption features to the point of non-detection, making σ_* difficult to determine directly. Shields et al. (2003) pioneered using the FWHM of [O III] $\lambda 5007$ (divided by 2.35 under the assumption of a Gaussian profile) as a proxy for σ_* in luminous quasars. Others have since verified that FWHM [O III] $\lambda 5007$ does correlate, albeit with significant scatter, with σ_* (Boroson 2003; Gaskell 2009b), although the [O III] profile is not generally Gaussian and the relationship is not so simple. Brotherton (1996) found no relationship between FWHM [O III] $\lambda 5007$ and radio-based orientation indicators, although σ_* measurements may depend on the orientation to the line of sight of host galaxies disks (e.g., Woo et al. 2015).

Other investigations by Salvander et al. (2008) and Salvander & Shields (2013) used an $H\beta$ -based scaling relationships to determine the quasar black hole mass, and FWHM [O III]/2.35 as a proxy for σ_* , in order to study the M - σ_* relation using large samples of spectra from the Sloan Digital Sky Survey (SDSS). Notably, while they found M/σ_* significantly correlated with redshift, they accounted for most of the effect as the result of a variety of selection biases and argued that $M_{\text{BH}}-\sigma_*$ did not strongly evolve. They did not identify differences between radio-loud and radio-quiet quasars. We propose that much of their scatter in $M_{r_{\text{mBH}}}-\sigma_*$ arises from the orientation bias in FWHM $H\beta$, and that it may be possible to use scatter in the $M_{r_{\text{mBH}}}-\sigma_*$ relation computed in this way as an orientation indicator.

In the rest of this paper, we first recalibrate FWHM [O III] $\lambda 5007$ as a predictor of σ_* without assuming a Gaussian profile (§2.1). Then we construct a radio-loud quasar sample using the SDSS for which we can measure $M_{\text{BH}}-\sigma_*$ and compare it to radio-core dominance, an orientation indicator (§2.2). We calculate the correlation matrix for quantities of interest (§3), finding strong orientation effects as expected. We discuss prospects for, and challenges with, using our results to estimate orientation for quasars in general (§4). We also discuss the nature of a surprising new class of outliers having extremely broad emission lines but large radio core dominance that may be merger products (§4). Finally, we summarize our conclusions (§5).

2 SAMPLES, DATA, AND METHODS

2.1 Calibration of FWHM_[OIII] as a σ_* predictor

Instead of assuming a profile shape for the narrow [O III] $\lambda 5007$ emission line or relationship with the stellar velocity dispersion, we prefer to empirically calibrate FWHM_[OIII] as a predictor of σ_* . This has been previously done (e.g., Boroson 2003, Gaskell 2009b), but we can now do this with much larger samples with the same quality of spectra that we will work with throughout this investigation.

We started with the sample of Shen et al. (2008), who measured σ_* from stellar absorption lines in more than 900 broad-lined AGNs with spectra from the Sloan Digital Sky Survey (SDSS). Their measurements included corrections for instrumental resolution and aperture effects. They did not make any measurements of the narrow [O III] profiles, however.

We downloaded SDSS spectra for these objects and made our own measurements. Along with a local continuum

and an appropriately broadened Fe II template (Boroson & Green 1992), we fit [O III] $\lambda 5007$ and [O III] $\lambda 4959$ simultaneously with a fixed 3:1 intensity ratio, using the same profile comprised of the sum of two skewed Gaussians with different peak wavelengths allowed to vary. This mathematical function satisfactorily reproduced the full range of observed [O III] profiles in the sample. From these analytical fits, we numerically determined the FWHM. We obtained the instrumental resolution at the wavelength of [O III] $\lambda 5007$ from the SDSS headers and subtracted this in quadrature from the observed FWHM to determine an intrinsic FWHM. This is an important step because the smallest FWHM values are not much larger than the intrinsic spectral resolution.

We determined errors using an empirical formula based on Monte Carlo simulations. We created a grid of artificial [O III] profiles with a range in signal-to-noise ratios and equivalent widths spanning those seen in our data set. For each grid point, we created 50 artificial spectra with random Gaussian noise added at different levels and measured profile properties. The distribution of measurements provides the uncertainties for the grid. We then employed multiple regression using signal-to-noise ratio and equivalent width as predictors of the uncertainty and used the resulting fit to determine individual error bars. The mean uncertainty on our final FWHM [O III] measurements was $11\pm 3\%$.

We excluded a number of objects for several reasons. Upon visual inspection, some spectra had poor signal-to-noise ratios or other spectral defects in the region of [O III] compromising our fits. Some spectra show double-peaked [O III] profiles, which are of interest as binary candidates (e.g., Fu et al. 2011), but which are unlikely to be representative of typical line profiles and might skew our work. A few spectra would not properly download from the SDSS servers. Our final sample consists of 773 objects. Table 1 provides our new measurements of FWHM [O III] along with σ_* with uncertainties and aperture corrections from Shen et al. (2008).

Figure 1 plots \log FWHM [O III] against the \log of the aperture-corrected stellar velocity dispersion σ_* . Objects with radio flux densities greater than 10 mJy at 1.4 GHz with the NRAO VLA Sky Survey (NVSS, Condon et al. 1998) and within $30''$ of the SDSS position (as recommended by Kimball & Ivezić 2008) are distinguished by filled circles. With only 17 objects, the filled circles do not differ at a statistically significant level from the open circles, and we conclude that there is no strong dependence on radio-loudness. We also note that [O III] profiles are not Gaussians, and that FWHM [O III]/2.35 generally underpredicts σ_* , as shown on the plot, and should not be used.

The quantities \log FWHM [O III] and $\log \sigma_*$ are strongly correlated, with a Spearman correlation coefficient of 0.53, which is extremely significant with 773 points. Care must be taken when choosing a method of fitting a line in the presence of scatter, keeping in mind the intended application of the fitted relationship. The appropriate line fit to predict one parameter from another in an unbiased manner is the ordinary least squares (OLS) Y on X line (e.g., Isobe et al. 1990). Unbiased here means that the residuals between the y parameter and the fitted line do not correlate with the x parameter. The OLS Y on X line shown on to predict $\log \sigma_*$ based on \log FWHM [O III], all in km s^{-1} is:

Table 1. Measurements for the revised Shen et al. (2008) sample. The full table is available online.

SDSS Name (J2000)	z	σ_* (km s ⁻¹)	Corr σ_* (km s ⁻¹)	FWHM [O III] (km s ⁻¹)	Inst. res (km s ⁻¹)	Intrinsic FWHM [O III] (km s ⁻¹)
000611.54+145357.2	0.1186	181.1±13	189	344.8	136.2	316.8±36
000729.98−005428.0	0.1454	121.2±18	128	269.3	132.3	234.6±27
000805.62+145023.3	0.0455	173.1±8	173	407.6	146.1	380.6±38
000813.22−005753.3	0.1393	221.8±18	233	475.8	133.1	456.8±36
001255.02+010905.2	0.1547	140.5±24	148	311.8	143.0	277.1±33
001340.21+152312.0	0.1196	92.4±14	96	265.2	128.0	232.2±30
001903.17+000659.1	0.0727	118.9±8	121	252.6	139.0	210.8±27
001954.35+155740.3	0.0828	98.8±9	101	259.2	127.9	225.5±28
002305.03−010743.4	0.1661	170.5±18	180	364.0	138.1	336.7±38
002839.65+145138.8	0.1963	69.4±17	74	238.8	144.3	190.4±30

$$\log \sigma_{*[OIII]} = 1.0366(\pm 0.0712) + 0.4701(\pm 0.0284) \log \text{FWHM}[OIII] \quad (1)$$

Extra digits are provided in the fitting parameters for plotting purposes. This produces a distribution of y-axis residuals centered on zero as desired for prediction, with a standard deviation of 0.12 dex, or about 30%.

The OLS Y on X line, especially when significant scatter is present, can differ from more symmetric approaches to fitting. A line fit that treats the x and y axes symmetrically is more appropriate when trying to determine the underlying relationship between two variables. Given that this may be of interest, we also provide the OLS Y on X and OLS X on Y bisector fit:

$$\log \sigma_* = -0.12252(\pm 0.0323) + 0.9332(\pm 0.0126) \log \text{FWHM}[OIII] \quad (2)$$

We generated the 1σ uncertainties for the above equation with a Monte Carlo approach, using the observed parameter distributions and 1000 iterations.

2.2 Radio-Loud Sample and Measurements

We can use the radio core dominance parameter, determined from radio maps of our sources, to estimate jet orientation in quasars. The Shen et al. (2008) sample only includes ~ 50 objects with radio detections in FIRST (Becker et al. 1995), many of which are not formally radio-loud. Using the [O III] $\lambda 5007$ FWHM to predict σ_* , we constructed a much larger sample from the SDSS more suitable for our purposes.

We started with the Shen et al. (2011) SDSS DR7 quasar catalog and selected objects that have $z < 0.75$ to ensure good measurements of [O III] $\lambda 5007$ and the $\lambda 5100 \text{ \AA}$ continuum used for SE black hole mass scaling relationships. We also only selected objects with $i < 19.1$, where SDSS is nearly complete, and for which the signal-to-noise ratio is not too low to make good spectral measurements.

Next, we cross correlated this sample with the NRAO VLA Sky Survey (NVSS, Condon et al. 1998), keeping matches with flux density $S_{1.4} > 10$ mJy and within $30''$ of the SDSS position (as recommended by Kimball & Ivezić 2008). The selection criteria ensures radio measurements well above the detection limit of both NVSS and FIRST and reliable matches. At lower redshifts, however, this flux

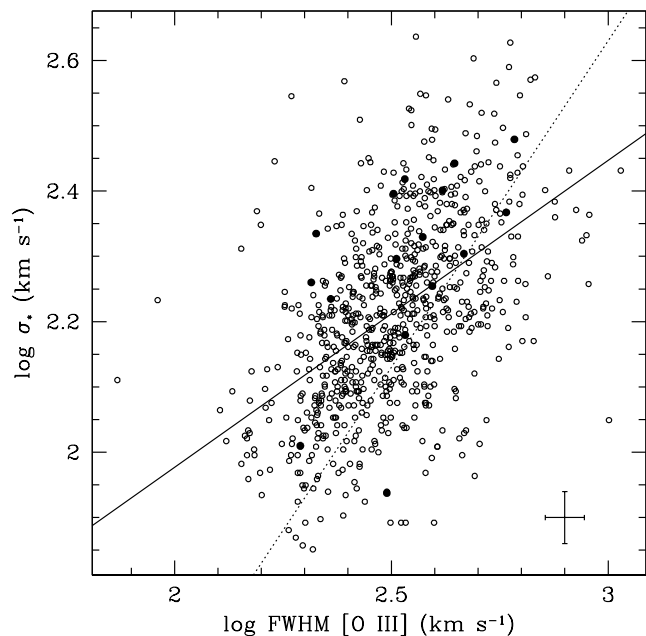


Figure 1. We plot $\log \text{FWHM [O III]}$ against $\log \sigma_{*[OIII]}$ for our final sample of 773 objects, with the filled circles indicating the 17 sources detected in the radio with 1.4 GZ flux density $S_{1.4} > 10$ mJy. The solid line is the OLS Y on X regression line of equation 1. The dotted line shows the equation for $\sigma_* = \text{FWHM [O III]}/2.35$.

density limit does not fully exclude radio-quiet quasars. An additional criterion of the Shen et al. (2011) radio loudness parameter $RL > 10$ removes the handful of remaining radio-quiet objects. We also required that the slope parameter of the continuum of H β region have $\alpha_\lambda < -0.5$ to eliminate any quasars with significant optical reddening, which would make them appear more intrinsically radio-loud than they actually are. Then we considered the position of the FIRST radio core compared to the optical SDSS position, removing objects from our sample that had mismatches greater than $2''$; when the FIRST radio cores and the optical positions do not match, the radio core flux density likely represents a peak, or significant contamination, from extended radio emission, which would result in a misleading measurement

of radio core dominance. Finally, we visually inspected the FIRST maps of all the remaining sources in order to identify extended radio lobes (see, e.g., Kimball & Ivezić 2008).

This selection procedure produced a final sample of 386 radio-loud quasars. We then measured the radio core dominance by computing the ratio of FIRST peak flux density to that of the extended emission (adding all the extended radio components together). We k-corrected these values to 5 GHz rest frame under the assumption that radio cores have a flat spectrum ($S_\nu \propto \nu^0$) and that extended radio emission has a steep spectrum ($S_\nu \propto \nu^{-0.7}$), resulting in our final core dominance measurements expressed as log R. While this procedure will yield reliable core dominance measurements for the majority of our sample, we must provide some caveats. As correctly pointed out and characterized by Jackson & Browne (2013), the spatial resolution of the FIRST survey (5'') is too low to resolve some radio sources, particularly those at higher redshifts. While our selection criterion of matching SDSS and FIRST positions helps, there will still be a number of poorly resolved sources that may cause problems, particularly in the case of Compact Steep Spectrum (CSS) sources (e.g., O’Dea 1998). Kimball & Ivezić (2008) estimate about 25% contamination from CSS and Gigahertz Peaked Sources (GPS) among compact radio sources. We note that when using log R for orientation, this contamination will create extra scatter among core-dominant sources but should not artificially create correlations that don’t exist. The systematic uncertainties involved with equating log R with orientation angle may dominate over formal measurement errors, which are typically about 0.15 dex.

Table 2 gives the optical properties of our radio-loud sample, many provided by the catalog Shen et al. (2011). The measurements of the FWHM [O III] profile are new and were done in the same manner as in §2.1. The estimate of σ_* uses equation 1. Table 3 provides core and extended radio properties from the FIRST Survey as described above, as well as our adopted radio core dominance parameter k-corrected to 5 GHz rest-frame. Table 4 provides some statistical properties of the tabulated parameters that may be of interest.

3 ANALYSIS AND RESULTS

Our primary interest is using the radio core dominance log R in order to test how quantities involved in the $M\text{-}\sigma_*$ relation, as computed using quasar proxies, depend on orientation. Some dependence, especially on black hole mass computed from $H\beta$, is expected, and likely contributes significant scatter. It may also be possible to use ratios of black hole mass computed with orientation-dependent and orientation-independent quantities to estimate orientation in quasars, whether or not radio loud. We also note that we are using a moderately large sample of radio-loud quasars that may turn up previously unrecognized rare objects.

Table 4 presents the Spearman rank correlation matrix for quantities of interest; Pearson correlation coefficients give similar results. To the quantities in tables 2 and 3, we add M_{σ_*} , the black hole mass computed from our $\sigma_{*[OIII]}$ using the $M\text{-}\sigma_*$ relationship from McConnell & Ma (2013), $\log M_\sigma = 8.32 + 5.64 \log(\sigma/200 \text{ km s}^{-1})$, which we use to create a normalized mass $M_{H\beta}/M_{\sigma_*}$. Below each correlation co-

efficient we give the two-sided probability of such a value arising by chance. Many highly significant correlations are present, and some notable non-correlations.

An inspection of the correlation matrix shows that $M_{H\beta}$ and σ_* , determined by their proxies, are significantly correlated, but the $M\text{-}\sigma$ relationship in this sample needs a closer look. Figure 2 plots $\log M_{H\beta}$ against $\log \sigma_*$ for the radio-loud sample (filled circles), and, in order to cover a wider range in parameter space to put our work in context, the objects from Shen et al. (2008) we used to develop equation 1 (open circles) using self-consistent measurements. We also show a line fit for the local quiescent galaxy $M\text{-}\sigma_*$ relation (McConnell & Ma 2013). Our selection criteria lead to the sample containing most luminous and massive systems at $z < 0.75$, which are not representative of the full range of quasar properties. The points for our sample sit well above the local $M\text{-}\sigma$ relationship, consistent with the work of Gaskell (2009b) and Salviander & Shields (2013) who used a similar approach employing similar proxies for mass and stellar velocity dispersion. They also found the most massive black holes shifted above the quiescent galaxy line. Being rare and luminous objects, our radio-loud quasars also sit at higher redshifts than the Shen et al. (2008) sample. The $M\text{-}\sigma$ relation for quasars in our individual and combined samples changes with z , as Salviander & Shields (2013) also found, and likely for the same reasons, involving a variety of selection biases, although they do not absolutely rule out true evolution.

Next, Figure 3 reproduces the log R – FWHM $H\beta$ plot of Wills & Browne (1986), again finding these quantities highly correlated in the sense that the more edge-on sources have the broadest lines on average. We note several differences, however. In particular, the upper right part of the figure is empty in Wills & Browne (1986) but has a small population of objects in our sample. This likely arises in part from contamination from CSS sources, but some of these quasars, when checked in NASA’s Extragalactic Database (NED), have radio spectra that are flat, not steep. We also note that our sample has few sources with $\log R < -1$, likely a result of excluding sources without close SDSS-FIRST core matches as well as the relatively high-frequency selection of FIRST and NVSS at 1.4 GHz; Wills & Browne (1986) use quasars mainly selected from low-frequency surveys that yield more lobe-dominant objects.

Figure 4 shows a plot of log of the mass ratio $M_{H\beta}/M_{\sigma_*}$ against log FWHM $H\beta$. This may be compared to a similar figure by Shen & Ho’s (2014), also Figure 4, where they plot the ratio of M_{σ_*} to the $H\beta$ virial product, the so-called “f-factor” used to empirically correct $H\beta$ -based masses for unknown geometric effects. The scatter in $M_{H\beta}/M_{\sigma_*}$ for a given FWHM is roughly consistent with that expected from the scatter in the proxies used to construct the ratio. Unlike Shen & Ho (2014), we do not see statistically significant improvement in the correlation if we create subsamples by binning in M_{σ_*} , perhaps because of our different parameter space and/or additional scatter from using FWHM [O III] as a proxy. In principle, M_{σ_*} should normalize the $H\beta$ -based mass, as neither FWHM [O III] nor the predicted σ_* are significantly correlated with log R, consistent with Brotherton (1996). We note that the average of the mass ratio is not unity, as we have already shown how the most massive quasars sit systematically above the local/quiescent galaxy

Table 2. Optical measurements for the radio-loud sample. The full table is available online.

SDSS Name	z	iMAG (mag)	logL5100 (erg s ⁻¹)	FWHM _{Hβ} (km s ⁻¹)	log M _{Hβ} (M _⊙)	log L/L _{Edd}	FWHM _[OIII] (km s ⁻¹)	log σ _* [OIII] (km s ⁻¹)
000111.19–002011.5	0.5179	–24.10	44.699 ± 0.007	5016.1 ± 584.6	8.66 ± 0.1	–1.09	470.8 ± 35	2.32±0.08
005905.51+000651.6	0.7189	–26.00	45.446 ± 0.007	4976.2 ± 1037.7	8.94 ± 0.13	–0.64	925.9 ± 62	2.46±0.08
005917.47–091953.7	0.6409	–24.16	44.795 ± 0.004	3653.9 ± 408.1	8.43 ± 0.1	–0.77	306.4 ± 21	2.24±0.08
010644.15–103410.5	0.4677	–24.54	44.907 ± 0.006	3355.4 ± 142.6	8.42 ± 0.04	–0.64	500.1 ± 30	2.33±0.07
012905.32–005450.5	0.7067	–24.95	45.132 ± 0.02	3020 ± 750	8.68 ± 0.12	–0.76	355.6 ± 39	2.27±0.10
013352.66+011345.1	0.3081	–23.39	44.461 ± 0.007	4205.1 ± 422.7	8.39 ± 0.09	–1.06	310.4 ± 27	2.22±0.08
021125.07–081440.3	0.5371	–23.88	44.645 ± 0.009	4672.5 ± 640.7	8.57 ± 0.12	–1.06	237.1 ± 32	2.18±0.11
021225.56+010056.1	0.5128	–24.43	44.805 ± 0.007	4945.3 ± 678.4	8.7 ± 0.12	–1.03	303.3 ± 17	2.23±0.07
030210.95–075209.4	0.7338	–24.93	44.966 ± 0.104	5380.6 ± 1249.2	8.56 ± 0.12	–0.8	187.6 ± 26	2.14±0.12
073320.83+390505.1	0.6637	–25.14	45.088 ± 0.019	2758.7 ± 265.5	8.34 ± 0.08	–0.38	697.7 ± 70	2.40±0.10

Table 3. FIRST 1.4 GHz measurements for the radio-loud sample and core dominance. The full table is available online.

SDSS Name	z	Core (mJy)	Extended (mJy)	K-corrected log R
000111.19–002011.5	0.5179	29.0	29.0	0.30
005905.51+000651.6	0.7189	2434.0	2434.0	1.19
005917.47–091953.7	0.6409	33.5	33.5	1.02
010644.15–103410.5	0.4677	269.0	269.0	0.28
012905.32–005450.5	0.7067	11.4	11.4	0.66
013352.66+011345.1	0.3081	16.7	16.7	–0.35
021125.07–081440.3	0.5371	32.9	32.8	1.18
021225.56+010056.1	0.5128	51.1	51.1	–0.02
030210.95–075209.4	0.7338	455.5	455.3	0.99
073320.83+390505.1	0.6637	130.5	130.5	0.93

M-σ_{*} relationship used to determine M_{σ_{*}}. If the M-σ-*** relationship is consistent for this sample, then mass variations cannot drive the correlation. The uncertainties on FWHM Hβ, which enter into quantities on both axes, are too small to drive the correlation. We therefore conclude, like Shen & Ho (2014) whose sample was primarily radio-quiet quasars, that a major part of the variation in FWHM Hβ arises from orientation effects, and that it is reflected in the M_{Hβ}/M_{σ_{*}} ratio.

Table 5 shows a highly significant correlation ($\sim 5\sigma$) between M_{Hβ}/M_{σ_{*}} and log R, which we plot in Figure 5. There is significant scatter, and caveats about the possible intrinsic variation in the M-σ_{*} relation apply, but we can again use the OLS Y on X regression line to predict log R from the orientation-biased mass ratio:

$$\log R = 0.797(\pm 0.0615) - 0.278(\pm 0.0584)\log M_{H\beta}/M_{\sigma_*} \quad (3)$$

Because of the large scatter, we would caution against using this relationship for individual quasars. Furthermore, because of the contamination of some fraction of expected CSS sources in the upper right portion of the distribution, which would have much smaller log R values if measured with a survey with higher spatial resolution than FIRST, the slope of the above equation is likely steeper in reality. VLA A-array observations of this sample would be helpful to correct for this contamination in a future investigation.

Finally, we performed one more experiment to test the orientation dependence of M_{Hβ}/M_{σ_{*}}. We computed a cor-

rected black hole mass, using equation 5 from Runnoe et al. (2013), that removed the orientation dependence from M_{Hβ} by adding $0.173 \times \log R$. Figure 6 repeats Figure 5, but uses this orientation-corrected black hole mass. Although there is still similar scatter, the accuracy is improved by removing orientation effects as the Spearman rank correlation coefficient is reduced from a highly significant -0.203 (two-tailed probability $< 0.01\%$ of arising by chance) to an insignificant -0.0004 (two-tailed probability of 99% of arising by chance). This test uses a different sample than Runnoe et al. (2013), and also a different way of normalizing the black hole mass (based on σ_{*} rather than the C IV λ1549 line), represents independent support for their mass correction term using log R. While it has been clear for some time that Hβ-based black hole mass determinations possess an orientation bias, we have now quantified the effect and provided additional evidence that we can correct for it, at least statistically.

4 DISCUSSION

Previous work and our results establish that black hole masses determined using the broad Hβ emission line suffer orientation bias, certainly in radio-loud quasars and very likely in radio-quiet quasars as well (e.g., Krolik 2001; Collin et al. 2006). Based on the investigation of Runnoe et al. (2013), this is also true using alternative velocity measurements like the line dispersion σ_{line} and true for Mg II λ2800, which behaves similar to Hβ. Quantitatively the bias is close to an order of magnitude over the observed full range of

Table 4. Statistical description of the radio-loud sample

Property	Mean	SEMean	Standard Deviation
z	0.51	0.008	0.15
iMag	-24.45	0.046	0.91
log L ₅₁₀₀	44.85	0.02	0.37
log FWHM H β	3.73	0.01	0.23
log M _{Hβ}	8.80	0.03	0.52
log M _{σ_*}	7.92	0.02	0.38
log L/L _{Edd}	-1.08	0.02	0.46
log FWHM [O III]	2.59	0.007	0.15
log $\sigma_{*[\text{O III}]}$	2.25	0.003	0.07
log R	0.55	0.035	0.69

Table 5. Spearman Rank Correlation Coefficients and Probabilities

	z	L ₅₁₀₀	FWHM H β	M _{Hβ}	L/L _{Edd}	FWHM [O III] or σ_*	M _{Hβ} /M _{σ_*}
L ₅₁₀₀	0.590						
	<0.0001						
FWHM H β	0.093	0.155					
	0.068	0.002					
M _{Hβ}	0.303	0.496	0.898				
	<0.0001	<0.0001	<0.0001				
L/L _{Edd}	0.090	0.173	-0.918	-0.716			
	0.0786	0.0006	<0.0001	<0.0001			
FWHM [O III] or σ_*	0.074	0.192	0.167	0.225	-0.079		
	0.147	0.0001	0.001	<0.0001	0.12		
M _{Hβ} /M _{σ_*}	0.222	0.319	0.724	0.773	-0.619	-0.382	
	<0.0001	<0.0001	<0.0001	<0.0001	<0.0001	<0.0001	
log R	-0.088	-0.061	-0.271	-0.248	0.248	0.003	-0.203
	0.086	0.235	<0.0001	<0.0001	<0.0001	0.959	<0.0001

quasar orientations, and represents a significant amount of scatter in many applications (e.g., studying M- σ_* as in Salviander & Shields 2013). There is no reason to think that reverberation mapping black hole masses are immune from orientation effects, although this would be good to confirm observationally.

Orientation also affects optical luminosity (e.g., Nemmen & Brotherton 2010, Runnoe et al. 2013, and references therein), which can manifest in numerous ways. For instance, flux-limited samples possess strong orientation biases that can change the slope and normalization of quasar luminosity functions (e.g., DiPompeo et al. 2014). We agree with the conclusions of Shen & Ho (2014) that orientation is an important parameter affecting the appearance of type 1 quasars, above and beyond being a primary reason for type 1 and type 2 AGNs more generally (e.g., Antonucci 1993).

As a practical matter, having multiple estimators for quasar black hole mass, that can be computed without radio observations and that have different dependencies on orientation, offers the promise of an orientation indicator that can be used in all quasars, radio-loud and radio-quiet alike. Such a general orientation indicator could be used to look for orientation bias, as well as to correct for its effects.

The ratio of an orientation-biased black hole mass to one derived from an unbiased stellar velocity dispersion σ_* , or a reasonable proxy like FWHM [O III], can serve as a rough orientation indicator. There remain issues to consider besides the scatter. The intrinsic M- σ_* ratio may vary

with AGN type, the host galaxy type, the black hole mass, and perhaps redshift as well (in addition to discussions by Gaskell 2009b and Salviander & Shields 2013, see also Benkert et al. 20011, Kormendy & Ho 2013, Woo et al. 2015, and others). One additional issue we propose here is an orientation effect with luminosity. If ideas about a receding torus and a correlation between luminosity and opening angle are correct (e.g., Lawrence 1991; Ma & Wang 2013), then more luminous quasars will be on average seen at larger viewing angles. This in turn will mean that they will on average have larger FWHM H β and therefore correspondingly larger black hole mass estimates when using H β single-epoch scaling relationships. This effect could contribute to more luminous quasars also sitting higher in M- σ diagrams like our Figure 2. These topics are of course of great interest and study in their own right.

Because of the large amount of scatter between these parameters, this predictive equation is unlikely to be reliable for determining orientation in individual objects. However, given the large numbers of quasars now being routinely studied, it may prove useful for statistical studies. There may also be opportunities to improve the relationship and reduce scatter.

We previously discussed some caveats associated with the use of the FIRST survey to determine radio core dominance. Certainly there are some compact steep spectrum quasars that would have small values of log R if observed at higher spatial resolution, but are interpreted as jet-on

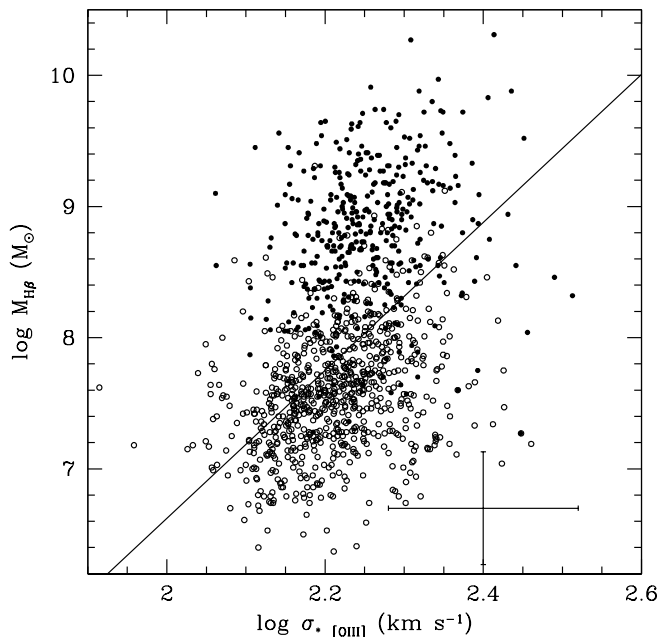


Figure 2. We plot $\log M_{H\beta}$ against $\log \sigma_{*}$ relation for our radio-loud sample (filled circles) using estimates of these parameters from the SE black hole mass scaling relationship using $H\beta$ (VP06) and equation 1. The representative error bar displayed represents the scatter in the predictive equations rather than measurement errors, which are very much smaller. For reference, we have also plotted the objects from Figure 1 (open circles), which are on average lower redshift and luminosity, using for consistency the same proxies to estimate mass and velocity dispersion. The line shown is a recent update for the local M - σ_{*} relation in quiescent galaxies (McConnell & Ma 2013).

quasars with large core dominance. This effect creates extra scatter in Figures 3 and 5. A fraction of our sample has additional radio measurements available from the Westerbork Northern Sky Survey at 325 MHz (WENSS, Rengelink et al. 1997). Some of the objects with both large $\log R$ and $\text{FWHM } H\beta$ that sit in the upper right corner of Figure 3, an empty area in the plot of Wills & Browne (1986), do indeed have steep radio spectra. Some, however, have flat spectra and probably do indeed represent jet-on systems.

If the scenario of Wills & Browne (1986), proposing that $H\beta$ is emitted from a disc-shaped BLR in the plane perpendicular to the jet axis, is right, how could some of these jet-on systems show the broadest $H\beta$ lines of all? For example, SDSS J161826.93+081950.7 has $\log R = 1.76$ and a flat radio spectrum, but also $\text{FWHM } H\beta = 24,000 \text{ km s}^{-1}$, one of the broadest broad emission lines ever seen in a quasar. Suggestive is the fact that the [O III] profile has a bump on the blue side, indicating that it is perhaps double-peaked, which has been previously noted by, e.g., Smith et al. (2010) and Fu et al. (2011), who included the quasar as a binary candidate. We propose that these rare objects, with apparently misaligned jet and BLR axes, could result from recent mergers. That is, a merger has already occurred and changed the system spin axis seen on large scales vs. small scales. Thus we see the large scale radio structure as indicating a jet-on orientation, but the broad line region is more

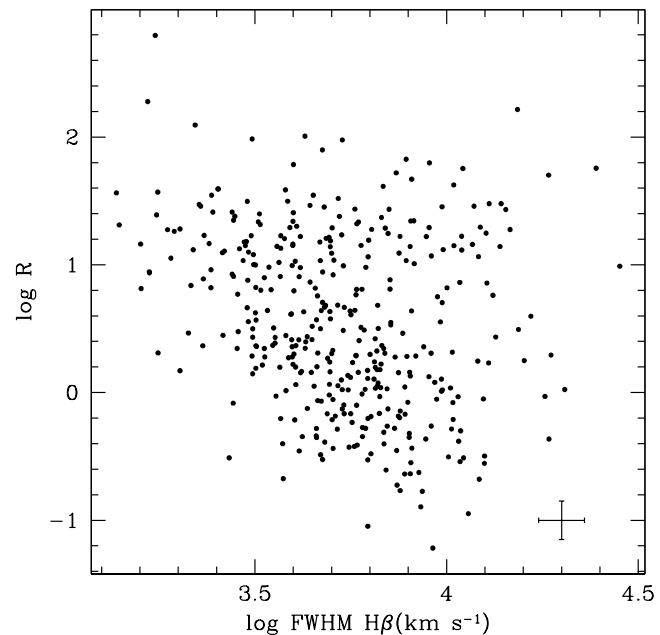


Figure 3. $\log R$ is plotted against $\log \text{FWHM } H\beta$. The uncertainties on $\log R$ are likely dominated by systematic issues as discussed in the text and are not always well determined, while the uncertainties on $\log \text{FWHM } H\beta$ are ~ 0.04 dex, very small compared to the sample parameter range.

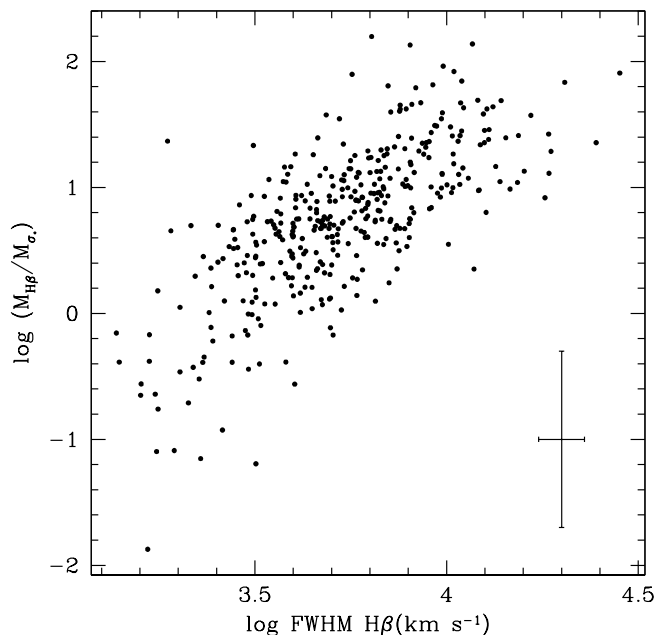


Figure 4. The $\log (M_{H\beta}/M_{\odot})$ is plotted against $\log \text{FWHM } H\beta$. The typical error bar is shown, where the magnitude for the y-axis represents scatter in the predictive relationships, and in the x-axis measurement errors.

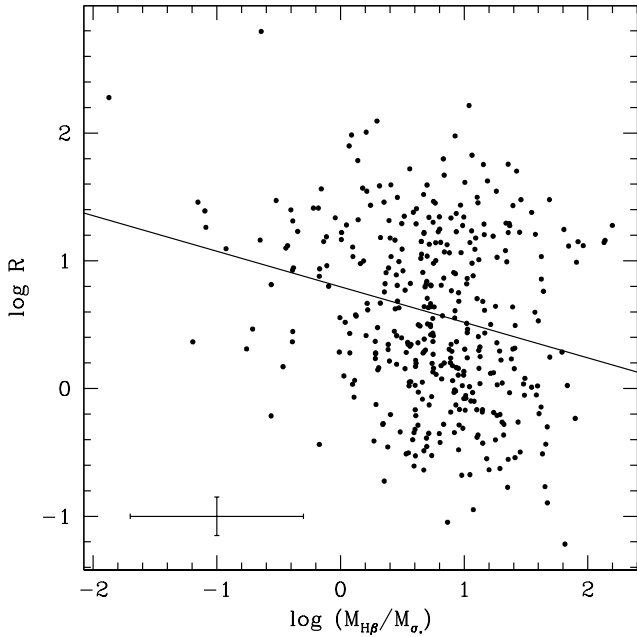


Figure 5. The log of $M_{H\beta}/M_{\sigma_*}$ is plotted against $\log R$, with uncertainties on $M_{H\beta}/M_{\sigma_*}$ again coming from scatter of the predictive equations. The Spearman rank correlation coefficient is -0.204 with a two-tailed probability of arising by chance of $< 0.01\%$. The solid line is the OLS Y on X regression line that may be used to predict $\log R$ from the orientation-biased to unbiased mass ratio.

edge-on. Follow-up investigations of the jets on millarcsecond scales with VLBI would be of interest.

5 SUMMARY

We recalibrated FWHM [O III] as a proxy for σ_* using the sample and measurements of Shen et al. (2008). We then constructed a sample of radio-loud quasars based on a combination of SDSS, NVSS, and FIRST catalogs and measured FWHM [O III] in order to predict σ_* . We found that single-epoch scaling relationship estimates of black hole mass using $H\beta$ appear to be strongly correlated with radio-based orientation indicators, even when normalized by mass determinations from the M - σ_* relation, consistent with some previous work. We discussed using the ratio of biased quasar black hole mass to stellar velocity dispersion as an orientation indicator, as well as a small population of outliers with both large $\log R$ and FWHM $H\beta$, which may represent recently merged systems.

ACKNOWLEDGMENTS

We thank Zhaohui Shang and Bev Wills for useful discussions, and the referee Martin Gaskell for helpful suggestions. Support for Vikram Singh came from Wyoming EPSCoR Undergraduate Research Fellowship Program and NSF Grant EPS-1208909.

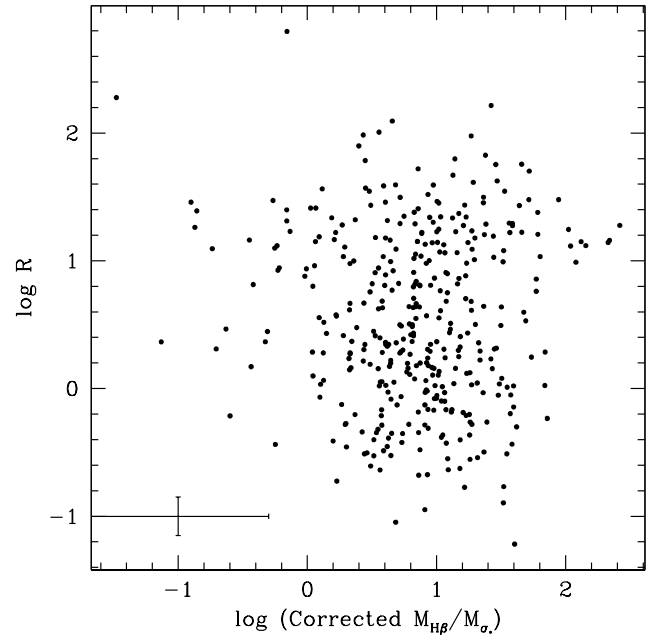


Figure 6. The log of $M_{H\beta}/M_{\sigma_*}$ is plotted against $\log R$, although this time $M_{H\beta}$ has been corrected for orientation bias using equation 5 from Runnoe et al. (2013). The Spearman rank correlation coefficient is -0.0004 , with a two-tailed probability of arising by chance of 99%, indicating the variables are not correlated.

REFERENCES

- Antonucci R., 1993, *ARA&A*, 31, 473
 Becker R. H., White R. L., Helfand D. J., 1995, *ApJ*, 450, 559
 Bennert V. N., Auger M. W., Treu T., Woo J.-H., Malkan M. A., 2011, *ApJ*, 742, 107
 Boroson T. A., 2003, *ApJ*, 585, 647
 Boroson T. A., 2011, *ApJ*, 735, LL14
 Boroson T. A., Green R. F., 1992, *ApJS*, 80, 109
 Brotherton M. S., 1996, *ApJS*, 102, 1
 Collin S., Kawaguchi T., Peterson B. M., Vestergaard M., 2006, *A&A*, 456, 75
 Condon J. J., Cotton W. D., Greisen E. W., Yin Q. F., Perley R. A., Taylor G. B., Broderick J. J., 1998, *AJ*, 115, 1693
 DiPompeo M. A., Myers A. D., Brotherton M. S., Runnoe J. C., Green R. F., 2014, *ApJ*, 787, 73
 Ferrarese L., Merritt D., 2000, *ApJ*, 539, L9
 Fu H., Myers A. D., Djorgovski S. G., Yan L., 2011, *ApJ*, 733, 103
 Gaskell C. M., 2009a, *NewAR*, 53, 140
 Gaskell C. M., 2009b, *arXiv*, arXiv:0908.0328
 Gebhardt K., et al., 2000, *ApJ*, 539, L13
 Isobe T., Feigelson E. D., Akritas M. G., Babu G. J., 1990, *ApJ*, 364, 104
 Jackson N., Browne I. W. A., 2013, *MNRAS*, 429, 1781
 Kimball A. E., Ivezić Ž., 2008, *AJ*, 136, 684
 Krolik J. H., 2001, *ApJ*, 551, 72
 Kormendy J., Ho L. C., 2013, *ARA&A*, 51, 511
 Lawrence A., 1991, *MNRAS*, 252, 586

- Ma X.-C., Wang T.-G., 2013, MNRAS, 430, 3445
McConnell N. J., Ma C.-P., 2013, ApJ, 764, 184
Nemmen R. S., Brotherton M. S., 2010, MNRAS, 408, 1598
O’Dea C. P., 1998, PASP, 110, 493
Orr M. J. L., Browne I. W. A., 1982, MNRAS, 200, 1067
Peterson B. M., 2011, arXiv, arXiv:1109.4181
Rengelink R. B., Tang Y., de Bruyn A. G., Miley G. K.,
Bremer M. N., Roettgering H. J. A., Bremer M. A. R.,
1997, A&AS, 124, 259
Runnoe J. C., Brotherton M. S., Shang Z., Wills B. J.,
DiPompeo M. A., 2013, MNRAS, 429, 135
Runnoe J. C., Brotherton M. S., DiPompeo M. A., Shang
Z., 2014, MNRAS, 438, 3263
Salviander S., Shields G. A., Gebhardt K., Bernardi M.,
Hyde J. B., 2008, ApJ, 687, 828
Salviander S., Shields G. A., 2013, ApJ, 764, 80
Shen J., Vanden Berk D. E., Schneider D. P., Hall P. B.,
2008, AJ, 135, 928
Shen Y., 2013, BASI, 41, 61
Shen Y., et al., 2011, ApJS, 194, 45
Shen Y., Ho L. C., 2014, Natur, 513, 210
Shields G. A., Gebhardt K., Salviander S., Wills B. J., Xie
B., Brotherton M. S., Yuan J., Dietrich M., 2003, ApJ,
583, 124
Smith K. L., Shields G. A., Bonning E. W., McMullen
C. C., Rosario D. J., Salviander S., 2010, ApJ, 716, 866
Sulentic J. W., Marziani P., Zamfir S., Meadows Z. A.,
2012, ApJ, 752, LL7
Van Gorkom K. J., Wardle J. F. C., Rauch A. P., Gobeille
D. B., 2015, MNRAS, 450, 4240
Vestergaard M., Peterson B. M., 2006, ApJ, 641, 689
Wills B. J., Brotherton M. S., 1995, ApJ, 448, L81
Wills B. J., Browne I. W. A., 1986, ApJ, 302, 56
Woo J.-H., Yoon Y., Park S., Park D., Kim S. C., 2015,
ApJ, 801, 38